

## Hippocampal replay of extended experience

Thomas J. Davidson, Fabian Kloosterman and Matthew A. Wilson

### Supplementary Figures (page 1-9)

Figure 1: Position estimation error

Figure 2: Neural decoding, replay detection and significance testing

Figure 3: Replay trajectory locations

Figure 4: Replay examples for rat 1

Figure 5: Replay examples for rat 2

Figure 6: Replay examples for rat 3

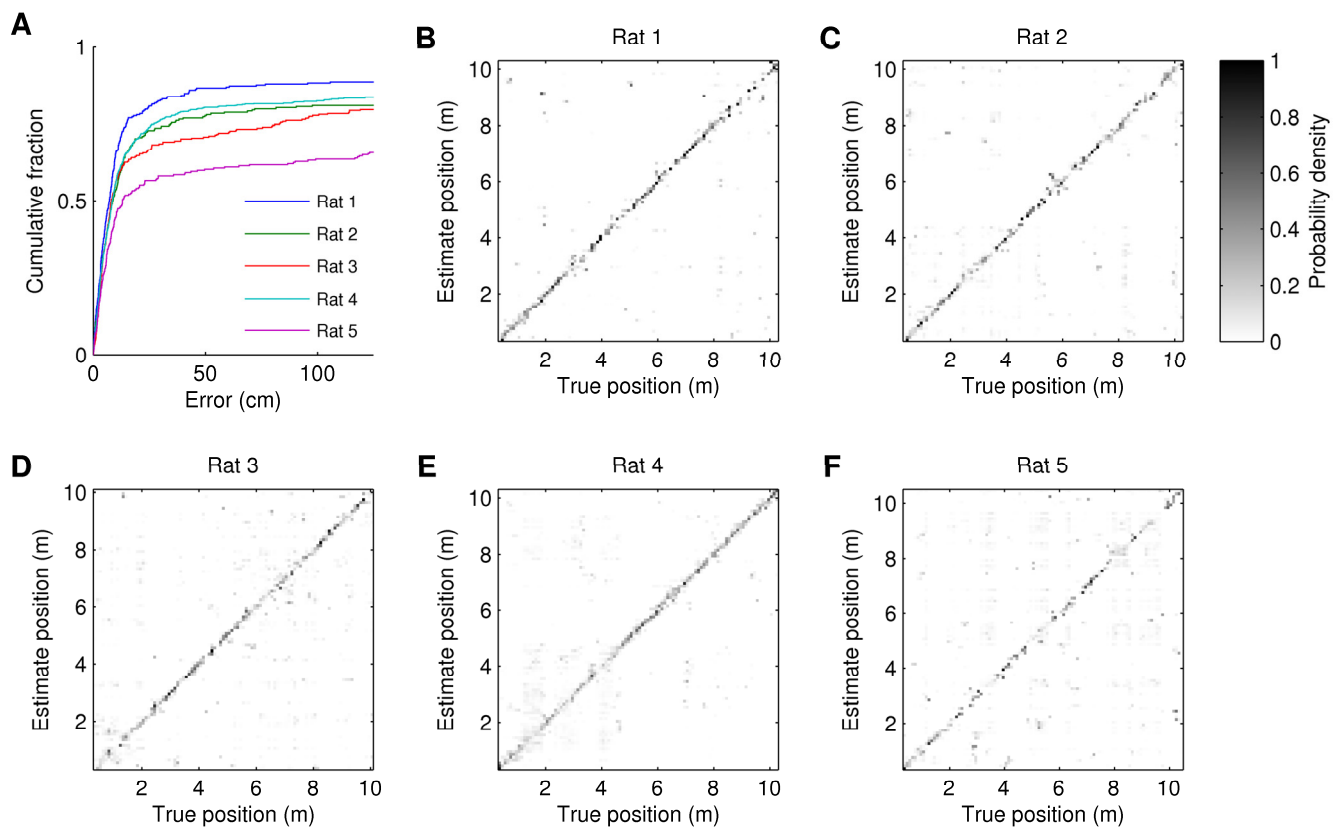
Figure 7: Replay examples for rat 4

Figure 8: Clustering and place fields for a single well-isolated unit

Figure 9: Theta sequences

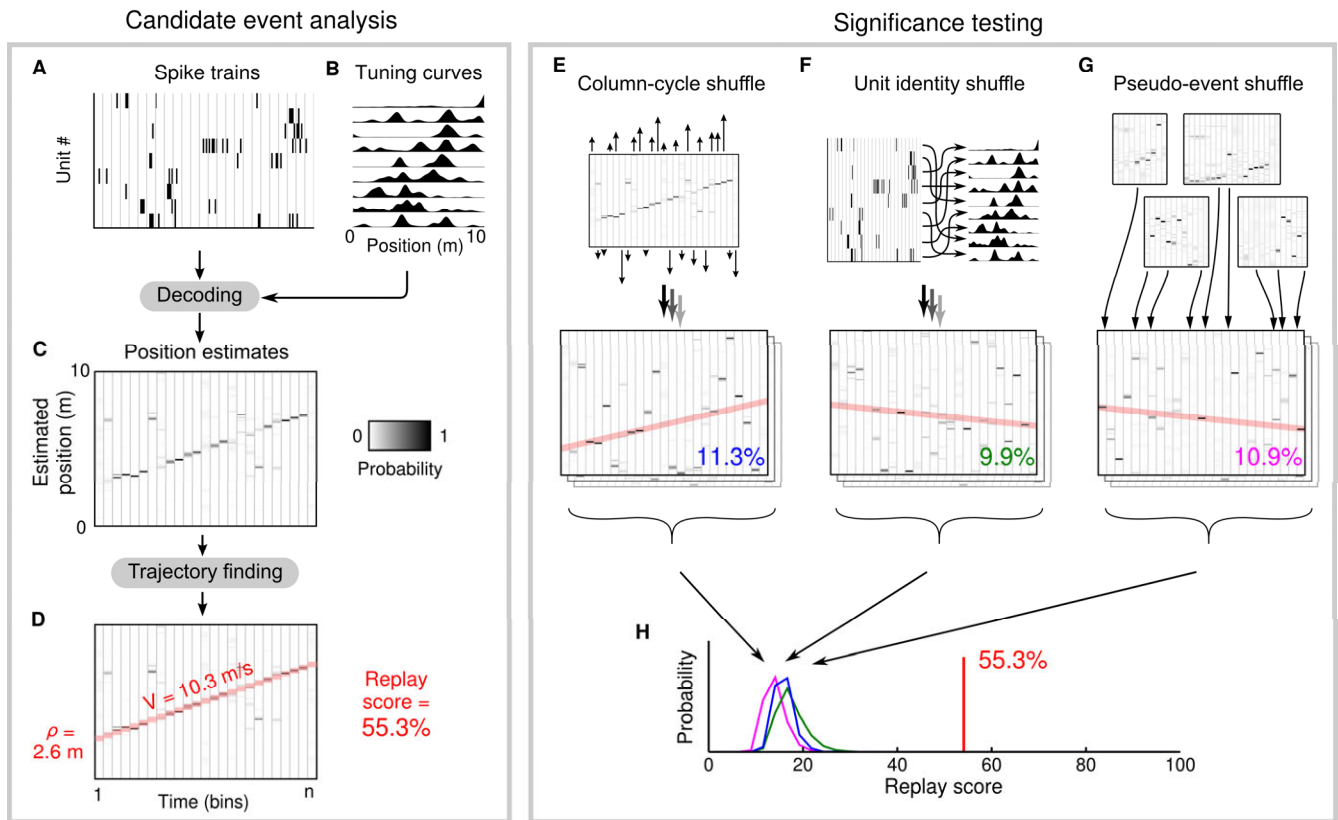
### Supplementary Results (page 10)

### Supplementary Methods (page 11-14)



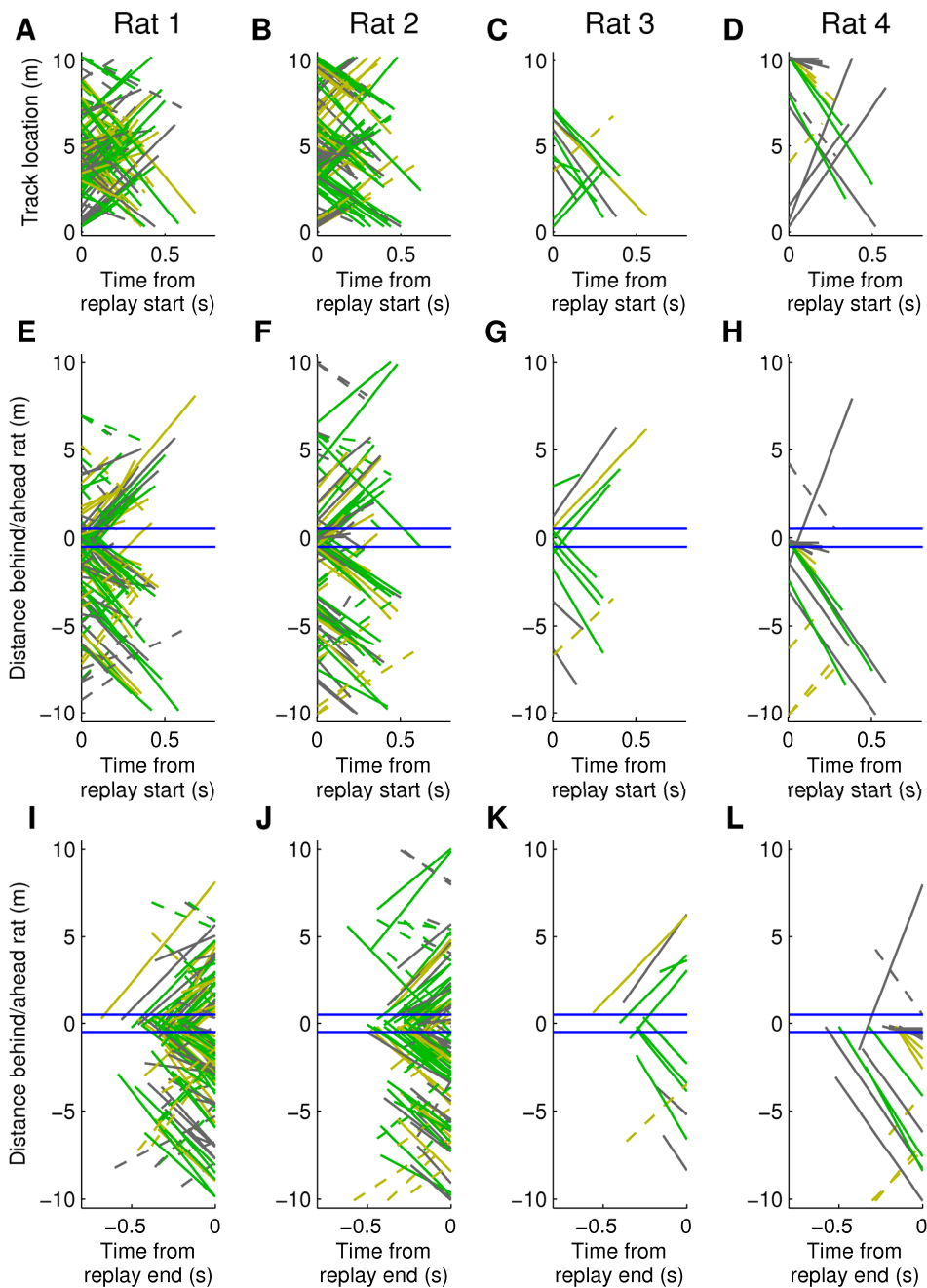
### Supplementary Figure 1: Position estimation error

Error measures for position estimation during RUN for rats 1-5 (500 ms time bins; test set validation). **A**, Cumulative distribution functions of the error of the maximum likelihood estimate of position **B-F**, Confusion matrices for rats 1-5. Each column corresponds to the average estimated probability distribution over position for a given true position (10 cm bins). Systematic estimation errors (i.e. 'confusing' one location for another) would appear as power off the identity diagonal. Notice that for animals 1-4 we can accurately estimate the rat's position for most locations on the track. Rat 5 was excluded from replay analysis due to poor reconstruction quality during RUN.



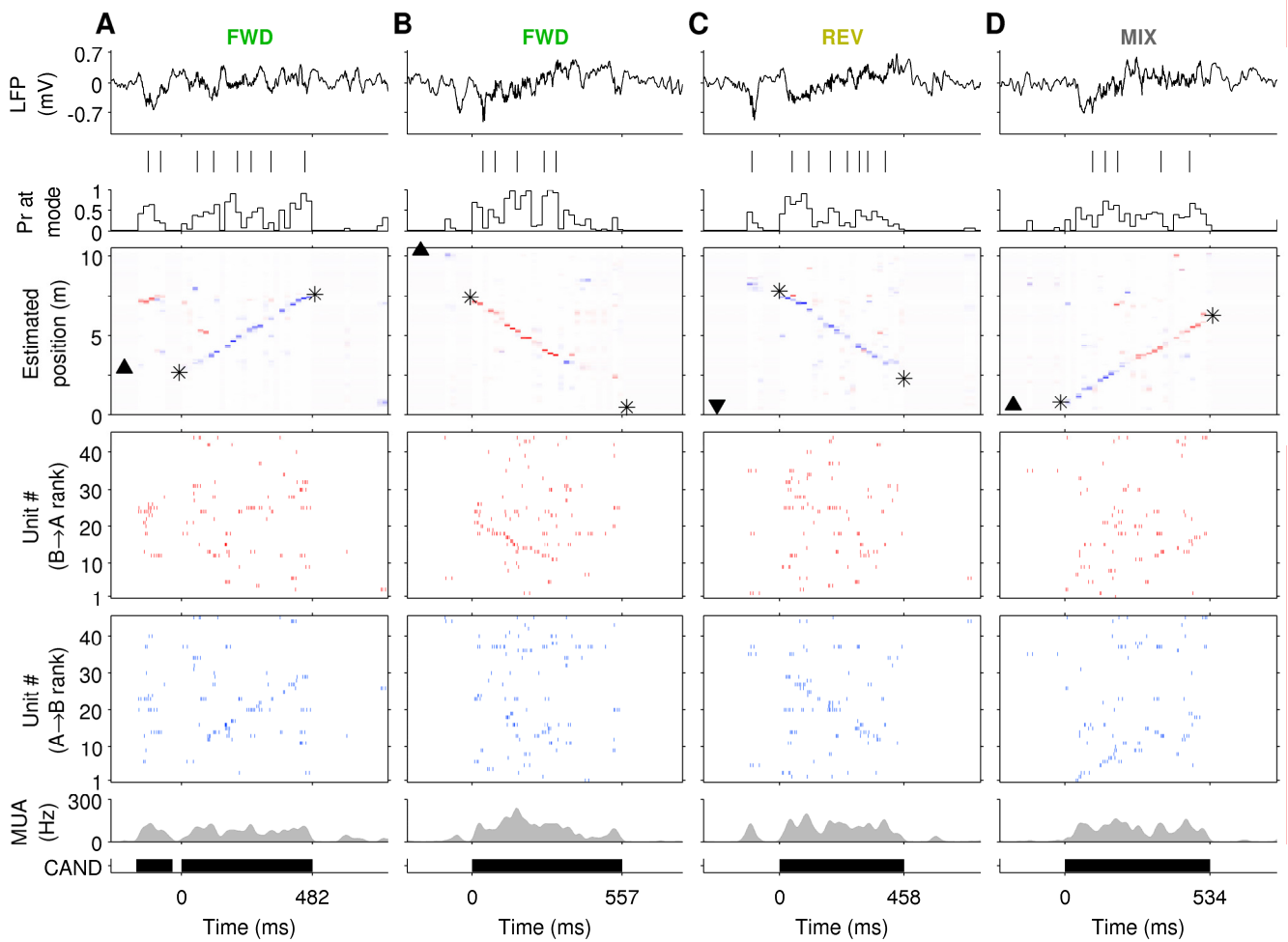
## Supplementary Figure 2: Neural decoding, replay detection and significance testing

**A-D**, Neural decoding and replay detection for a single candidate event. Spiking activity is divided into non-overlapping 20 ms bins (A). We estimate position within each time bin by decoding the ensemble activity using the spatial tuning curves (B) obtained during RUN. This gives an estimated probability distribution over position (PDF) for each time bin (plotted as columns in panel C). Replay appears as a systematic shift of the peak in the PDFs over time. To detect linear replay trajectories, we densely sample all possible lines (30 cm wide) and for each line compute a score equal to the mean likelihood that the rat was on the specified trajectory throughout the event. The line with the highest score (red shaded line in D) is selected as the candidate replay trajectory, and its score is reported as the 'replay score' for the event. **E-G**, The statistical significance of a candidate replay trajectory is assessed by repeating the scoring procedure on shuffled versions of the same data. **E**, In the 'column-cycle' shuffle, the PDF at each time bin is circularly shifted by a random distance. **F**, In the 'unit identity' shuffle, the mapping from each unit's spiking record to its spatial tuning curve is randomly permuted. **G**, The 'pseudo-event' shuffles are constructed by substituting each PDF in a candidate event for a PDF drawn at random from any other candidate event. **H**, Each type of shuffle is repeated 1500 times for each event to obtain three sample distributions. The true replay score (red line) is compared with each of these distributions, and the largest of the 3 resulting Monte-Carlo p-values is conservatively reported as the significance level for the event.



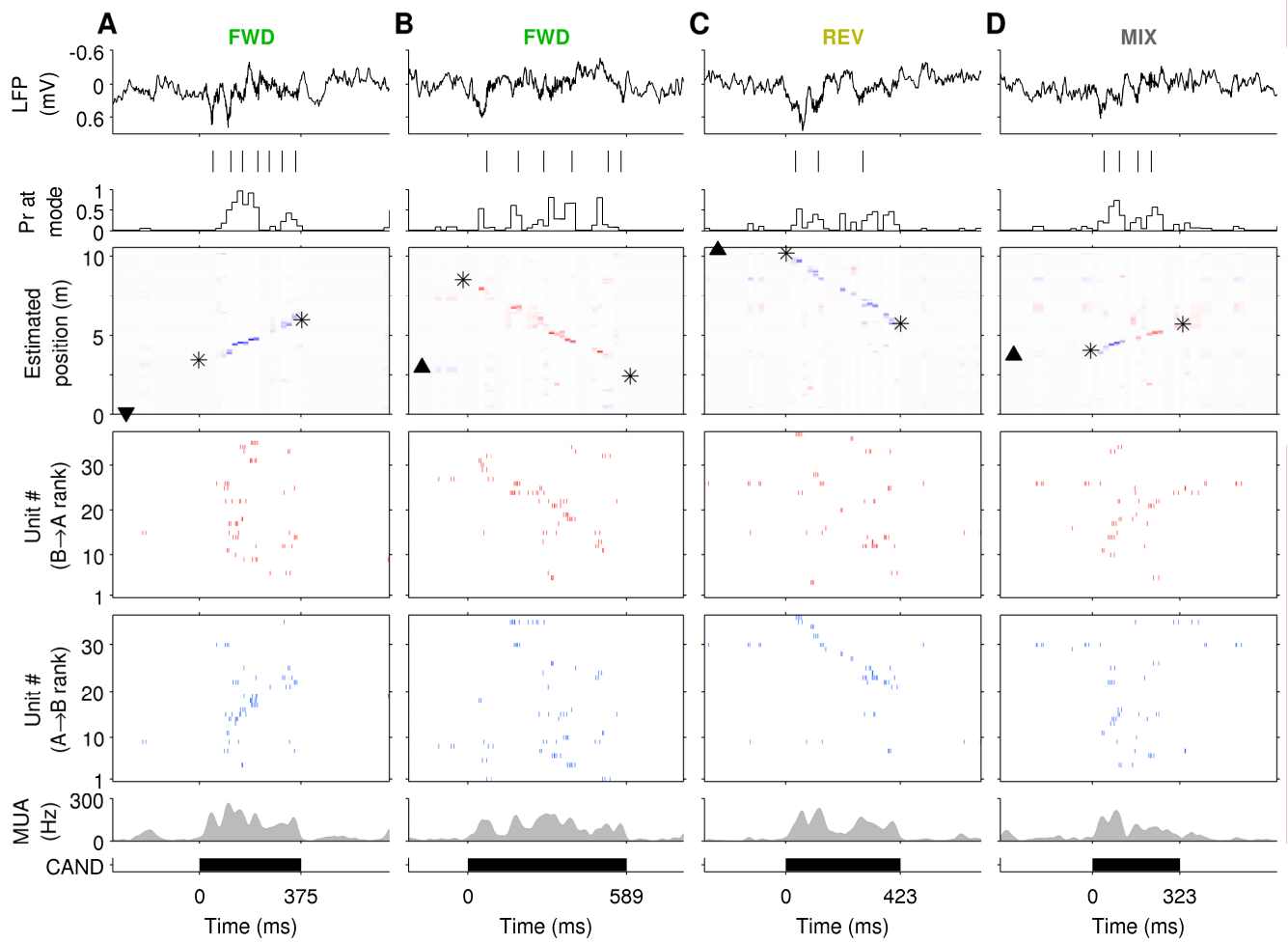
### Supplementary Figure 3: Replay trajectory locations

**A-D**, Significant ( $p < 0.01$ ) replay trajectories, aligned to the start time of the replay event. Note that replay can begin and end at any location on the track, not only at reward locations. Green: forward replay; yellow: reverse replay; gray: mixed replay; dashed lines: strictly remote replay (see text). **E-L**, The same replay trajectories as in A-D, but plotted relative to the animal's location at the time of the replay (positive distance values = locations ahead of the animal along the track; negative distance values = behind the animal). Replays plotted aligned to replay start (E-H) or end (I-L) time. Replay start locations, but not end locations, are significantly biased to start within 0.5 m of the current location (blue lines). Line colors as in A-D.



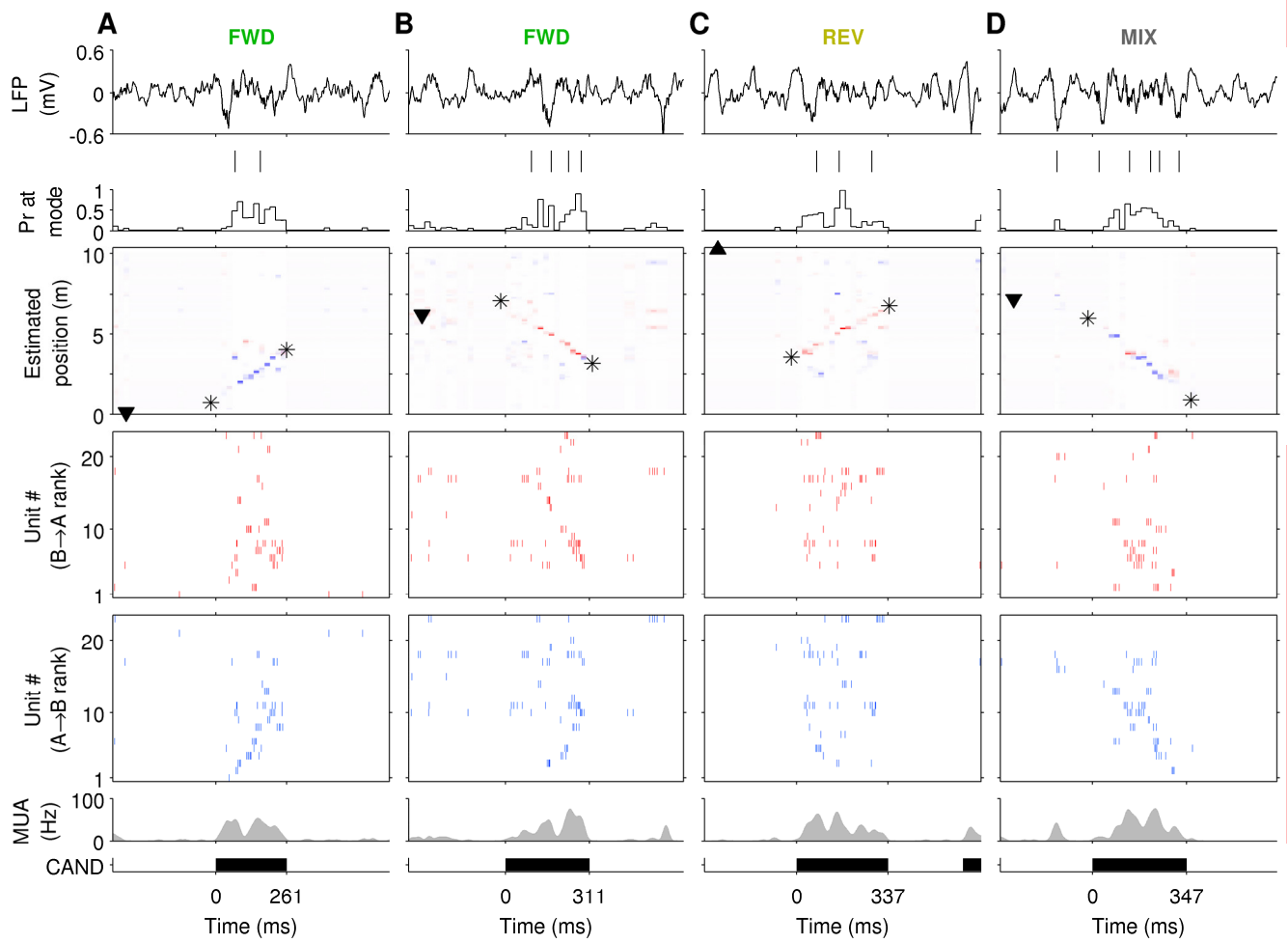
### Supplementary Figure 4: Replay examples for rat 1

**A-D**, Examples of candidate events containing forward (FWD), reverse (REV), and mixed (MIX) replay. For each example the following is shown (top to bottom): wide band LFP; detected ripples; mode of position reconstruction; position reconstruction; spike raster plot of all units sorted according to their preferred firing location when rat is running B→A direction; spike raster plot of all units sorted according to their preferred firing location when rat is running in A→B direction; Multi-unit activity across all tetrodes (MUA; average rate per tetrode including unclustered spikes); candidate event (CAND) start and end time. Black triangle in top panel indicates true location and facing direction of the rat throughout the event. Asterisks in top panel indicate start and end of detected replay trajectory. (Events are the same as those in Fig. 4B-E).



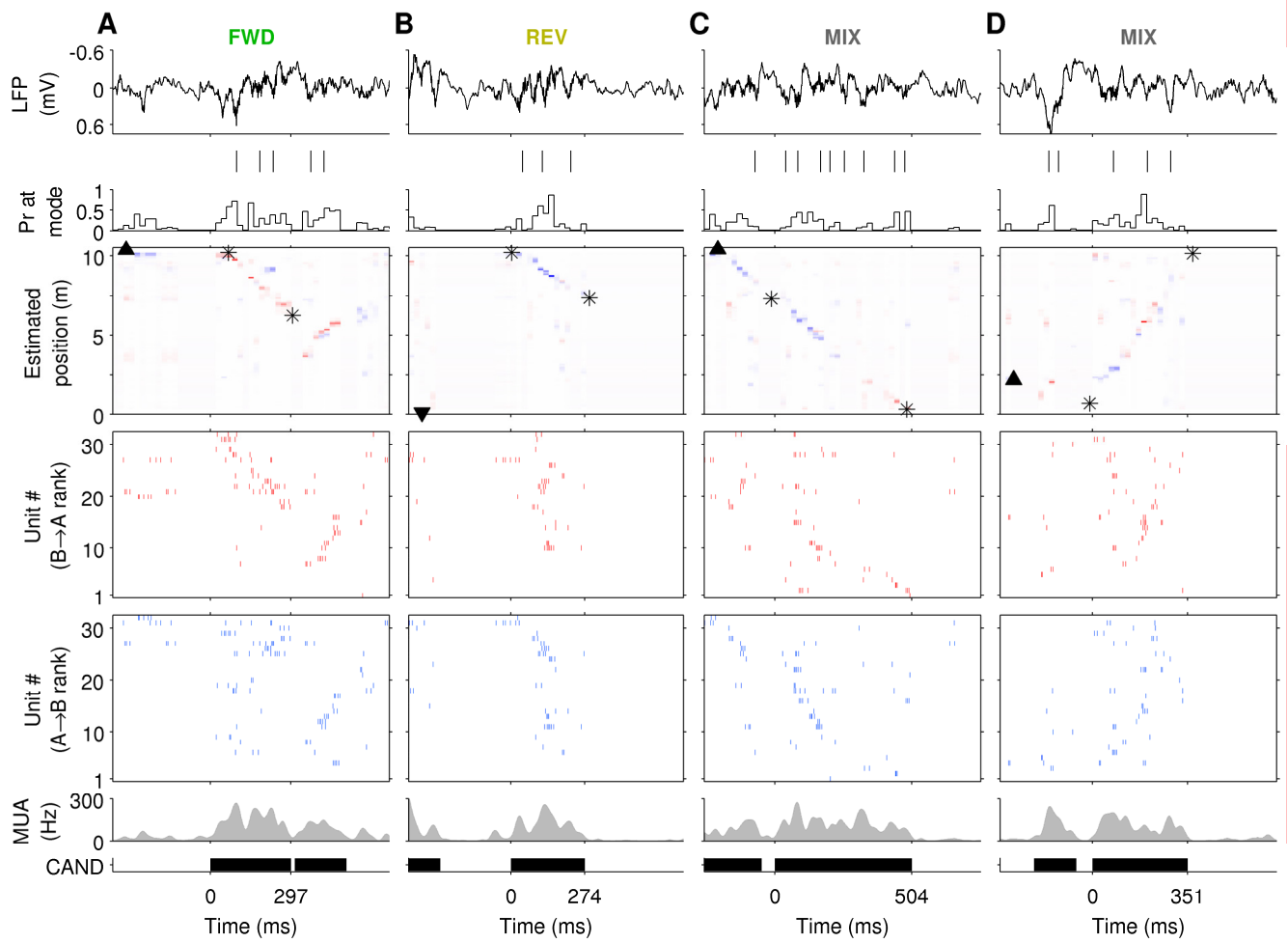
**Supplementary Figure 5: Replay examples for rat 2**

All panels as for Supplementary Fig. 4. LFP scale inverted to show sharp waves as downward-going.



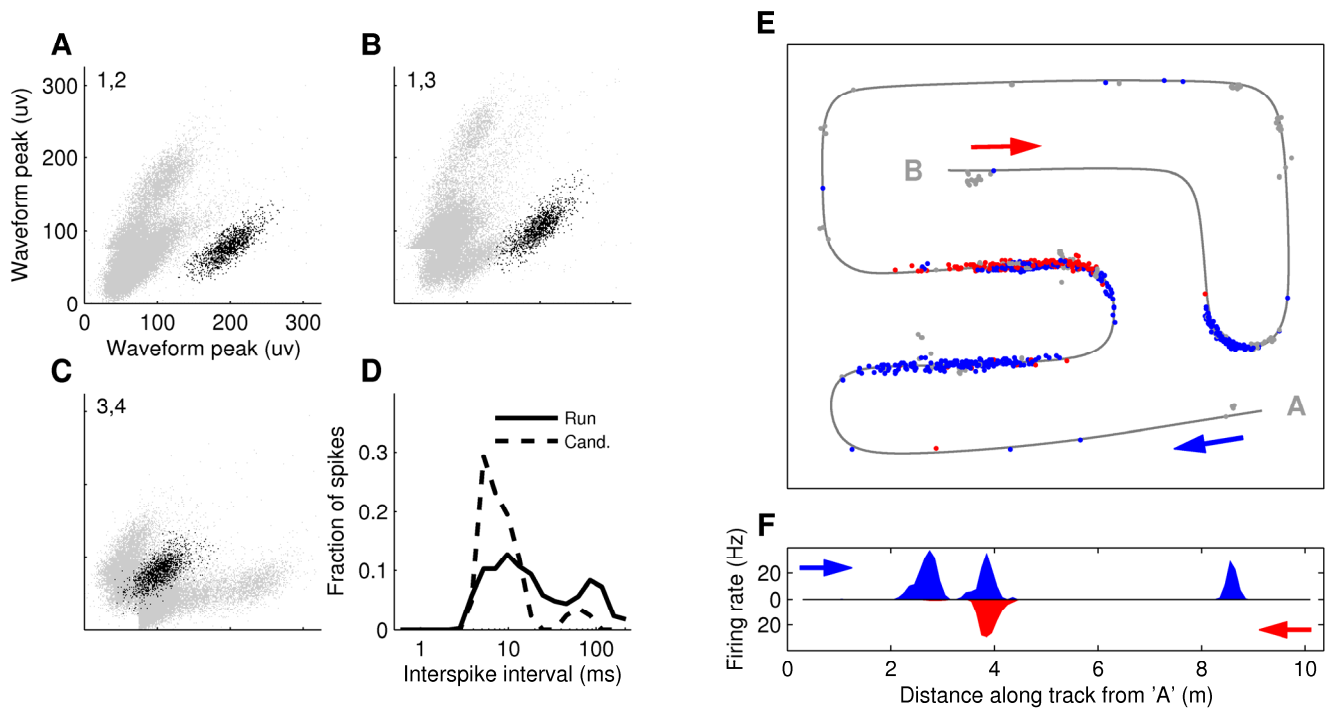
**Supplementary Figure 6: Replay examples for rat 3**

All panels as for Supplementary Fig. 4. LFP high-pass filtered (5 Hz cutoff) to remove movement artifacts.



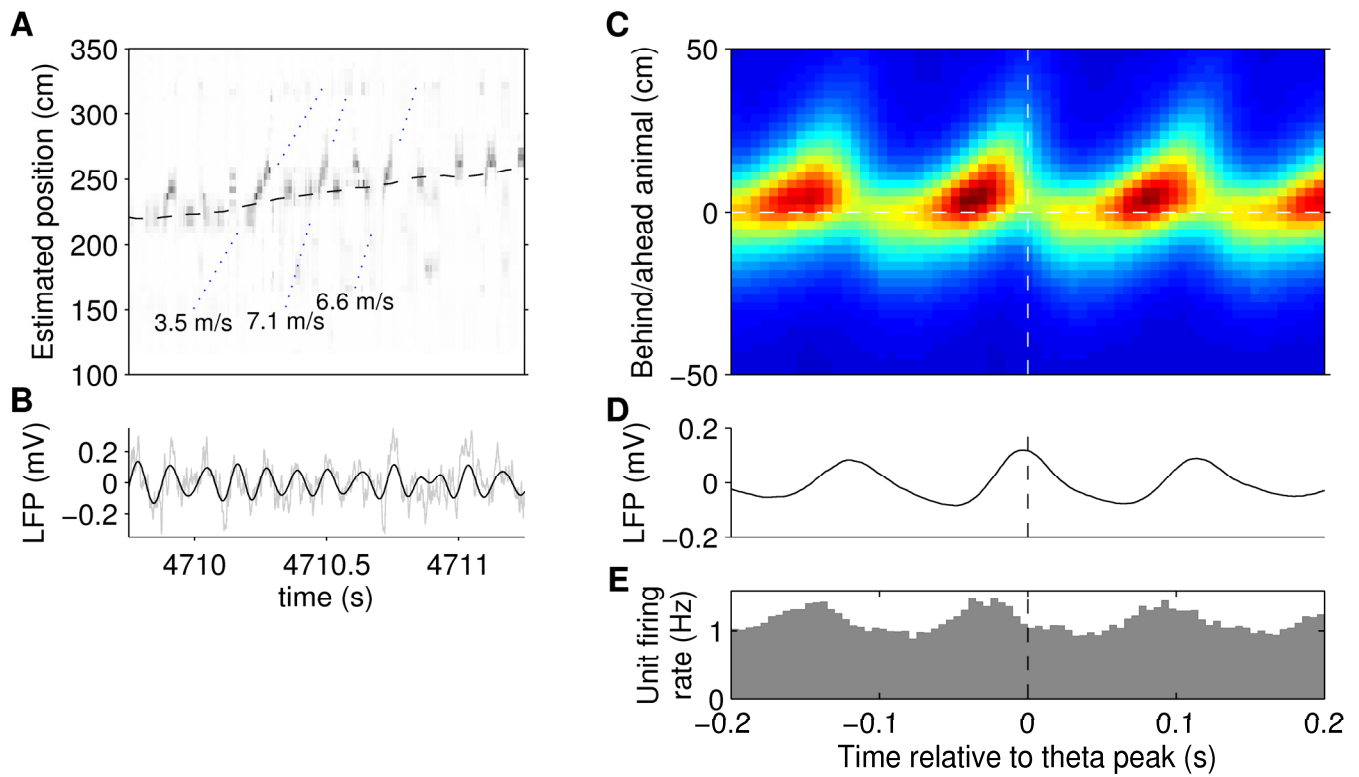
**Supplementary Figure 7: Replay examples for rat 4**

All panels as for Supplementary Fig. 4. LFP scale inverted to show sharp waves as downward-going.



**Supplementary Figure 8: Clustering and place fields for a single well-isolated unit.**

**A-C**, Scatter plots of peak waveform amplitude across pairs of channels for all spikes observed on a single tetrode. Black points represent spikes from a well-isolated unit. Tetrode channel numbers appear in top left of each panel. **D**, Inter-spike interval histogram during RUN and CAND events for the indicated unit, showing a clear refractory period as well as modulation at theta frequency during RUN. (Note log time scale.) **E**, Location of rat at all spike times for this unit. Blue: spikes emitted while rat was running A→B; red: spikes emitted while rat was running B→A; gray: spikes emitted when rat was not running. **F**, Joint tuning curve over linearized position and running direction. Blue: place-rate map during A→B runs; Red: place-rate map during B→A runs.



### Supplementary Figure 9: Theta sequences

Theta sequences are present in fine timescale position estimates (25 ms time bins, 75% overlap) calculated during RUN. **A**, Short sequences proceed ahead of the rat's true position (dashed black line). Selected slopes (blue dotted lines) are computed from a 62.5 ms period around zero-crossings of the theta oscillation. **B**, Raw (gray) and theta-filtered (black; 6-12 Hz bandpass) hippocampal LFP. **C-E**, Average theta sequence across all RUN periods. Theta-triggered averages of: rat-aligned position estimate (C); raw LFP (D), and mean firing rate per unit used in position estimates(E).

## Supplementary Results

### *Effect of unit isolation criteria on results*

We repeated all analyses performed in the paper using conservative unit isolation criteria (clear cluster boundary separation, clear refractory period in ISI, high complex-spike index [CSI], and low cross-CSI between clusters), obtaining between 17-32 simultaneously-recorded units with clear spatial modulation during behavior per session, rather than the 23-47 units used in the main paper.

The exclusion of marginally-isolated units resulted in a marked decrease in position decoding accuracy during RUN: median position error increased from 8.2 to 14.1 cm; the fraction of correct estimates of running direction decreased from 87% to 77%; and evenness of coverage over the long track was also poorer.

The same candidate event times were used since these depend only on unclustered multi-unit activity. Significant replay was detected in 8.6% of events, rather than the 16% we report in the main results (for events lasting at least 250 ms, the detection frequency was 20% rather than 33%). All results are significantly higher than the 1% expected by chance ( $p < 0.01$  per session,  $p < 10^{-13}$  pooled across sessions for both short and long events).

The characteristics of the detected replay were little changed. Median replay speed was 7.8 m/s rather than 8.1 m/s. Replay start locations remained significantly biased towards current location (39% local replay,  $p < 0.0005$ , rather than 40%). Remote replay accounted for 25% (rather than 20%) of detected events, and is observed significantly more frequently than expected by chance ( $p < 0.0001$  pooled across sessions). Replay order scores remained significantly biased towards forward and reverse ( $p < 10^{-47}$  pooled), and forward-ordered was more common than reverse-ordered replay (41% and 20% of all significant replay events, respectively, rather than 40% and 26%).

## Supplementary Methods

### *Position and running direction reconstruction*

We are interested in calculating the probability over the animal's position ( $pos$ ) and running direction ( $dir$ ) given a short time window of neural spiking ( $spikes$ ). According to Bayes' rule:

$$Pr(pos, dir|spikes) = \frac{Pr(spikes|pos, dir) \cdot Pr(pos, dir)}{Pr(spikes)} \quad (1)$$

We assume a uniform prior probability over position and direction,  $Pr(pos, dir)$ . Since the total probability must sum to 1, we therefore need only compute the likelihood,  $Pr(spikes|pos, dir)$ , in order to determine  $Pr(pos, dir|spikes)$ . Assuming the firing rates of all  $N$  units are independent, and assuming Poisson firing statistics we have:

$$Pr(spikes|pos, dir) = \prod_{i=1}^N Pr(spikes_i|pos, dir) \quad (2)$$

$$= \prod_{i=1}^N \frac{(\tau f_i(pos, dir))^{n_i}}{n_i!} e^{-\tau f_i(pos, dir)} \quad (3)$$

where  $\tau$  is the duration of the time window of observation,  $f_i(pos, dir)$  is the expected firing rate of the  $i$ -th unit as a function of position and direction (i.e. the tuning curve of the  $i$ -th unit), and  $n_i$  is the number of spikes emitted by the  $i$ -th cell in the time window. Combining equations (1) and (3) leads to the following result:

$$Pr(pos, dir|spikes) = C \left( \prod_{i=1}^N f_i(pos, dir)^{n_i} \right) e^{-\tau \sum_{i=1}^N f_i(pos, dir)} \quad (4)$$

where  $C$  is a normalization constant that depends on  $\tau$  and the number of spikes emitted by each cell. The output of this estimator is a 2-dimensional probability density function of location and running direction for the given time window. When only an estimate over position is required, we take the marginal of this distribution. When a point estimate is required, the location of the peak of the 2-dimensional distribution (i.e. the maximum likelihood estimate) is given.

We emphasize that, unlike the estimator used in Johnson and Redish (2007), our estimation algorithm is 'memoryless'. That is, the estimate depends only on spikes observed in the given time window, and not on any previous output of the estimator. Estimators that incorporate history perform better in decoding true location (Brown et al., 1998; Zhang et al., 1998), but are not well-suited to replay detection, since they would be expected to introduce spurious 'random walk'-like trajectories during random neural activity.

### ***Replay detection and significance testing***

To detect the constant-velocity trajectory that best describes the series of position estimates during a candidate replay event, we used a method similar to line finding in a 2-dimensional image, employing a modified discrete approximation to the Radon transform (Toft, 1996). Each trajectory is defined by its velocity ( $V$ ) and starting location ( $\rho$ ). For a candidate event consisting of  $n$  position estimates calculated at an interval of  $\Delta t$  (20 ms), the average likelihood  $R$  that the rat is within distance  $d$  of a particular trajectory is given by:

$$R(V, \rho) = \frac{1}{n} \sum_{k=0}^{n-1} Pr(|pos - (\rho + V \cdot k \cdot \Delta t)| \leq d) \quad (5)$$

(For those time bins  $k$  when a trajectory would specify a location beyond the end of the track, the trajectory is defined as specifying 'any location', and the median probability of all possible locations is taken as the likelihood). The value of  $d$  was empirically set to 15 cm to allow for detection of replays with small local variations in velocity.

To determine the most likely replay trajectory, we densely sampled the parameter space to find the values of  $V_{max}$  and  $\rho_{max}$  that maximize  $R$ . The value of  $R_{max}$  is a measure of the goodness-of-fit of the detected trajectory and is reported as 'replay score' for the candidate event (ranging between 0-100%).

To test whether the replay score for a particular event is higher than expected by chance, we compared it to the distribution of replay scores obtained after applying the same replay detection procedure to shuffled versions of the position estimates (Supplementary Fig. 2e-g). The shuffles tested were: 1) 'Column-cycle' shuffle: circularly shifting the estimate at each time bin by a random distance

(to control for chance alignment of locations along the trajectory); 2) 'Unit identity' shuffle: randomly permuting the mapping from spike trains to tuning curves (to control for patterns generated solely by spiking dynamics, such as static trajectories resulting from prolonged bursting of a single unit, or diagonal trajectories resulting from sequential bursting of any two units, etc.); and 3) 'Pseudo-event' shuffle: assembling 'pseudo-events' of identical duration to the original candidate events by making random draws of position estimates from other candidate events (to control for bias towards particular locations by the estimator). 1500 of each type of shuffle were performed for each event. Only candidate events with a Monte Carlo p-value (Davison and Hinkley, 1997)  $< 0.01$  for all shuffle types were classified as significant replay.

### ***Replay order scores***

For each candidate event containing significant replay a 'replay order' score is computed as the difference between the probabilities of running in the A→B and B→A directions, conditional on the position being on (within  $d$  cm of) the replayed trajectory. Thus for a candidate event consisting of  $n$  time bins, we can write:

$$\text{replay order} = \frac{\sum_{k=1}^n AB_k - BA_k}{\sum_{k=1}^n AB_k + BA_k} \cdot \text{sgn}(V_{max}) \quad (6)$$

where  $AB_k$  ( $BA_k$ ) is the probability that the position is on the trajectory and running direction is A→B (B→A) for time bin  $k$ . The replay order score has a value ranging from -1 to 1. The magnitude of the score reflects the degree to which the replayed trajectory is dominated by either of the directional representations, and the sign of the score reflects whether or not that dominant representation agrees with the direction of the replayed trajectory (positive; 'forward replay') or disagrees with it (negative; 'reverse replay'). Values close to zero indicate that on average both directional representations contribute equally ('mixed replay'). Pseudo-events used for significance testing were generated by drawing actual  $AB_k/BA_k$  pairs at random from all significant replay events within the same session.

### ***Theta-triggered position estimates***

Theta peaks were detected as local maxima in the band-pass filtered LFP (6-12 Hz) during all times the rat was running  $> 15$  cm/s. To detect the fine structure of theta sequences in Supplementary Fig. 9, position estimates were calculated for overlapping 15 ms time bins (5 ms steps) at a range of lags around each theta peak, then aligned according to the current position and running direction of the rat.

## References

Brown, E.N., Frank, L.M., Tang, D., Quirk, M.C., and Wilson, M.A. (1998). A statistical paradigm for neural spike train decoding applied to position prediction from ensemble firing patterns of rat hippocampal place cells. *J. Neurosci.* *18*, 7411-7425.

Davison, A.C., and Hinkley, D.V. (1997). *Bootstrap methods and their application* (Cambridge, UK ; New York, NY, USA: Cambridge University Press).

Johnson, A., and Redish, A.D. (2007). Neural ensembles in CA3 transiently encode paths forward of the animal at a decision point. *J. Neurosci.* *27*, 12176-12189.

Toft, P.A. (1996). *The Radon Transform - Theory and Implementation*. PhD thesis, Technical University of Denmark. URL: <http://petertoft.dk/PhD/>

Zhang, K., Ginzburg, I., McNaughton, B.L., and Sejnowski, T.J. (1998). Interpreting neuronal population activity by reconstruction: unified framework with application to hippocampal place cells. *J. Neurophysiol.* *79*, 1017-1044.